Seasonal Variability in Precipitation in Central and Southern Chile: Modulation by the South Pacific High

BRADFORD S. BARRETT

Oceanography Department, U.S. Naval Academy, Annapolis, Maryland, and Centro de Ciencias de la Atmósfera, Universidad Nacional Autónoma de México, Mexico City, Mexico

SULTAN HAMEED

School of Marine and Atmospheric Sciences, Stony Brook University, Stony Brook, New York

(Manuscript received 18 December 2015, in final form 15 June 2016)

ABSTRACT

Monthly precipitation in Chile (30°–55°S) was found to vary by intensity, latitude, and longitude of the South Pacific high (SPH). In austral winter, precipitation was higher when the SPH was weaker and when it was centered farther west. In austral spring, precipitation was higher when the SPH was weaker, similar to winter. However, spring precipitation was not found to be related to SPH longitude, and higher precipitation was found when the SPH was centered farther north. In austral summer, no relationship was found between precipitation and either SPH intensity or longitude, but positive correlations were found between precipitation and latitude of the SPH. In austral autumn, correlation patterns between precipitation and all three SPH metrics more closely resembled those seen in winter. The results of a multiple linear regression confirmed the importance of two SPH metrics (intensity and longitude) and the unimportance of a third SPH metric (latitude) in understanding variability in winter, summer, and autumn precipitation in central and southern Chile. In spring, regression results confirmed a relationship between precipitation and SPH intensity and latitude. Furthermore, the SPH intensity and longitude in winter combined to hindcast monthly precipitation with a better goodness of fit than five El Niño–Southern Oscillation metrics traditionally related to Chilean precipitation. Anomalies of lower-tropospheric circulation and vertical velocities were found to support the observed relationships between SPH and precipitation. Based on these results, a physical mechanism is proposed that employs the SPH as a metric to aid in understanding variability in precipitation in central and south-central Chile in all seasons.

1. Introduction

Precipitation in Chile varies on multiple temporal and spatial scales. Chile features a strong north–south precipitation gradient, with annual rainfall north of 30°S less than 100 mm increasing to over 3000 mm south of 40°S (Pizarro et al. 2012). Additionally, as elevation increases from sea level in the west to several thousand meters only a few hundred kilometers to the east, precipitation over the Andes Cordillera can be more than double that over the coast (Viale and Garreaud 2015). Seasonally, most of the rainfall in central and northern Chile (north of about 35°S) occurs in winter months (June–August), while south-central and especially southern Chile (south of 45°S) features precipitation nearly year-round (Montecinos et al. 2000; Garreaud 2009), with a transition zone in the middle. On the synoptic time scale, much of the rainfall in Chile originates from low pressure systems migrating eastward in the mid-latitude westerlies (Fuenzalida 1982), and between 30° and 40°S, this precipitation typically falls between late autumn and early spring (Montecinos and Aceituno 2003; Viale et al. 2013). Many of these low pressure centers bring cold fronts onshore, and convergence along these boundaries augmented by strong blocking of low-level flow from the Andes Cordillera results in significant precipitation along coastal and precordillera sites (Barrett et al. 2009). Indeed, Catto et al. (2012) found that between 40% and 80% of annual precipitation over central and southern Chile (30°–60°S) was attributable to frontal passages, with the fraction lowest

Corresponding author address: Bradford S. Barrett, Oceanography Department, U.S. Naval Academy, 572C Holloway Rd., Annapolis, MD 21402.
E-mail: bbarrett@usna.edu

DOI: 10.1175/JCLI-D-16-0019.1

around 30°S and highest around 60°S. Annual variability of the subtropical anticyclone in the South Pacific [also known as the South Pacific high (SPH); Grotjahn 2004], which migrates seasonally from about 28°S in winter to 35°S in summer, has been found to explain this annual rainfall cycle (wet in winter and dry in summer; Fuenzalida 1982). Analysis of the influence of the intensity and location of anticyclones on Chilean precipitation was pioneered by Pittock (1980), although he looked at surface pressures close to the Chilean coast and extending south to Antarctica and east into the South Atlantic. What is not yet well understood or quantified is the extent to which variability in the strength or position of the South Pacific anticyclone explains interannual variance in precipitation. Thus, the primary objective of this study was to explore the extent to which precipitation varied with surface pressures associated with the SPH.

One of the climate modes that has been well studied for its effects on precipitation in Chile is El Niño–Southern Oscillation (ENSO). On the interannual time scale, ENSO has been found to be moderately to occasionally strongly correlated with winter-season Chilean precipitation. For example, Rutllant and Fuenzalida (1991) found heavy precipitation events during El Niño episodes were associated with a wave train extending westward from Chile, and Karoly (1989) found this wave train was connected to anomalous convective heating in the tropical Pacific. Garreaud (1995) noted that large winter rain events in central Chile were characterized by either northward shifts in the storm track over the southeast (SE) Pacific or blocking to the southeast of Argentina that favored the quasi-stationary frontal systems over Chile. Aceituno (1988) found a robust relationship between precipitation in central Chile and an SST index over the central equatorial Pacific near 180°. ENSO-related variability is also seasonally dependent, with winter precipitation more favored during El Niño events from 30° to 35°S, while spring precipitation is more favored from 35° to 38°S and summer precipitation more favored south of 38°S, with about 80% of the variance in each region explained by the ENSO index (Montecinos 1998; Montecinos et al. 2000; Montecinos and Aceituno 2003). Rainfall in the Coquimbo region (approximately 29°–32°S) shows moderate relationship with an El Niño–Southern Oscillation index, with 32% of the variability in station-averaged rainfall from May to August explained by the index (Verbist et al. 2010). Despite these relationships, the extent of interannual variability of precipitation in Chile is complex, and long-period studies (e.g., of more than 50 years) have noted significant variability in the strength of the relationship between ENSO and Chilean precipitation (e.g., Aceituno and Montecinos 1993; Montecinos et al. 2000), suggesting that other sources of variability may act to control seasonal to interannual variability of precipitation.

Some aspects of the relationship between the SPH and El Niño–Southern Oscillation were explored by Grimm et al. (2000). They noted that during El Niño events, there is a consistent weakening of sea level pressures along the Chilean coast, resulting in an anomalous northward shift of the track of migratory low pressure systems. This result agrees with the case studies of Rutllant and Fuenzalida (1991) and results in greater precipitation in central and southern Chile. However, because a large fraction (40%–80%) of annual precipitation in central and southern Chile is associated with frontal passages (Catto et al. 2012), and because these frontal passages are related to variability in large-scale circulation features including the SPH (Viale and Nuñez 2011), it is critically important to directly explore the relationship between the SPH and precipitation. This present study fills that gap by exploring the seasonal relationship between precipitation and weighted-average sea level pressures over a large region of the South Pacific. The remainder of this paper is organized as follows: data and methodology are presented in section 2, results presented in section 3, and conclusions and suggestions for future work presented in section 4.

2. Data and methods

Monthly gridded precipitation observations from January 1980 to December 2013 were taken from the following three datasets: 1) the NOAA Climate Prediction Center (CPC) Merged Analysis of Precipitation (CMAP; Xie and Arkin 1997; data available online at http://www.esrl.noaa.gov/psd/data/gridded/data.cmap.html) dataset with 2.5° latitude by 2.5° longitude global spatial coverage; 2) the NOAA National Climatic Data Center (NCDC) Global Historical Climatology Network dataset, version 2 (GHCN; Peterson and Vose 1997; Chen et al. 2002; data available online at https://www.ncdc.noaa.gov/ghcnm/v2.php), a land-station-based dataset with 5° latitude by 5° longitude spatial coverage over land areas; and 3) the University of Delaware precipitation dataset, version 3.01 (Legates and Willmott 1990; data available online at http://www.esrl.noaa.gov/psd/data/gridded/data.UDel_AirT_Precip.html), a land-station-based dataset with 0.5° latitude by 0.5° longitude spatial coverage based, in part, on GHCN observations. We selected gridded precipitation products instead of station observations to focus on synoptic-scale variability and avoid any inhomogeneities that might arise from differing station period lengths and measurement practices. The three gridded datasets we selected capture similar structure in annual precipitation patterns (Fig. 1). For example, in all three datasets, the transition from arid northern Chile to

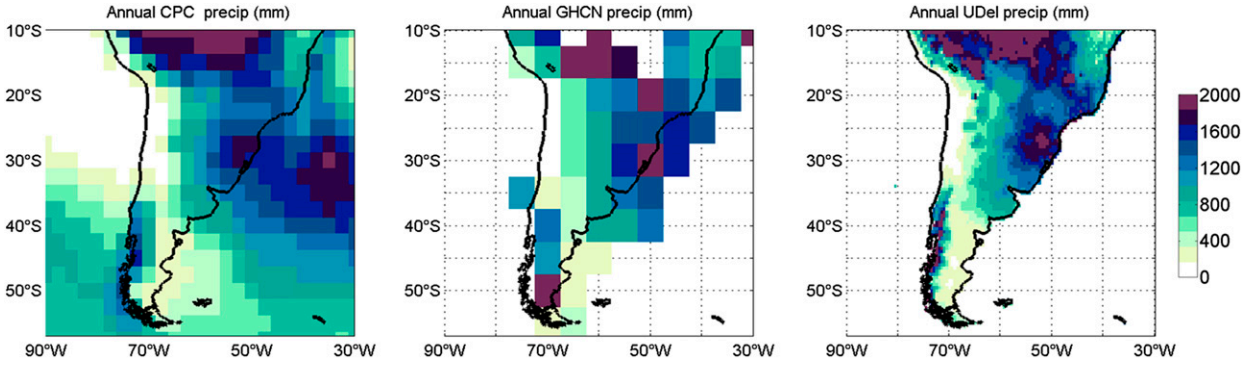

FIG. 1. Mean annual precipitation (mm) from (left) CMAP, (center) GHCN, and (right) University of Delaware gridded monthly datasets, from January 1980 to December 2013.

wet southern Chile is seen. Furthermore, seasonal variability in precipitation in central and southern Chile (from 30° to 60°S) is captured in all three datasets (Fig. 2).

Monthly averaged mean sea level pressure (MSLP) data from the National Centers for Environmental Prediction (NCEP)–National Center for Atmospheric Research (NCAR) reanalysis (Kalnay et al. 1996; data available online at http://www.esrl.noaa.gov/psd/data/gridded/data.ncep.reanalysis.html) on a 2.5° latitude by 2.5° longitude grid for 1980–2013 were used for calculating the indices for SPH intensity, SPH latitude, and SPH longitude. The pressure index I_p of the SPH is defined as an area-weighted pressure departure from a threshold value over the domain (I, J):

$$I_{p,\Delta t} = \frac{\sum_{i=1}^{I}\sum_{j=1}^{J}(P_{ij,\Delta t} - P_t)\cos\varphi_{ij}\delta_{ij,\Delta t}}{\sum_{i=1}^{I}\sum_{j=1}^{J}\cos\varphi_{ij}\delta_{ij,\Delta t}},$$

where $P_{ij,\Delta t}$ is the SLP value at grid point (i, j) averaged over a time interval Δt. The term P_t is a threshold SLP value ($P_t = 1016$ hPa for the SPH), and φ_{ij} is the latitude of the grid point (i, j). The term $\delta = 1$ if $(P_{ij,\Delta t} - P_t) > 0$ and $\delta = 0$ if $(P_{ij,\Delta t} - P_t) < 0$. This ensures that the pressure difference is due to the high pressure system. The intensity is thus a measure of the anomaly of the atmospheric mass over the section (I, J). Similarly, the SPH latitudinal index is defined as follows:

$$I_{\varphi,\Delta t} = \frac{\sum_{i=1}^{I}\sum_{j=1}^{J}(P_{ij,\Delta t} - P_t)\varphi_{ij}\cos\varphi_{ij}\delta_{ij,\Delta t}}{\sum_{i=1}^{I}\sum_{j=1}^{J}(P_{ij,\Delta t} - P_t)\cos\varphi_{ij}\delta_{ij,\Delta t}},$$

and the longitudinal index is defined in an analogous manner. The latitude and longitude of the SPH represent the location of the center of atmospheric mass over the domain. Seasonal average intensity, along with mean latitude and longitude locations of SPH centers, are shown in Fig. 3. The SPH is weakest in autumn (March to May; Fig. 4a) and also generally farthest west in autumn (Fig. 4b). The SPH is strongest in late winter and early spring (Fig. 4a) and is farthest east in summer (Fig. 4b). The SPH is farthest north in winter (June to August) and farthest south in summer (Fig. 4c).

Composites of monthly average MSLP, 10-m u- and v-vector wind components, 850-hPa vertical velocity in pressure coordinates (ω), and 850-hPa u- and v-vector wind components from the NCEP–NCAR reanalysis (Kalnay et al. 1996) were calculated to provide physical context to variability in the SPH. We also investigated possible physical relationships between the SPH and remotely located regions of diabatic heating, similar to the method of Leonardo and Hameed (2015) for the Hawaiian high. We selected the Climate Forecast System Reanalysis (CFSR; Saha et al. 2010; data available online at http://rda.ucar.edu/pub/cfsr.html) from 1980 to 2010 for that analysis. The CFSR uses a high-resolution fully coupled model and includes heating rates derived from condensation at multiple model levels, separated into three broad categories: 1) deep and 2) shallow convective heating rates and 3) large-scale condensate (Wright and Fueglistaler 2013). The large-scale condensate heating rate is a product of the model's cloud microphysical parameterizations and is associated with nonconvective processes. The other two heating rates are derived from cumulus parameterizations and separated into shallow and deep convection. If heating over a particular region contributes to subsidence over the South Pacific high, then there should be a positive correlation between the rates of heating and the SPH pressure.

Pearson product-moment correlations were calculated between monthly gridded GHCN precipitation and SPH intensity, latitude, and longitude to quantify the strength of variability of precipitation with the SPH's location and intensity (Fig. 5). Gridded precipitation over a subset

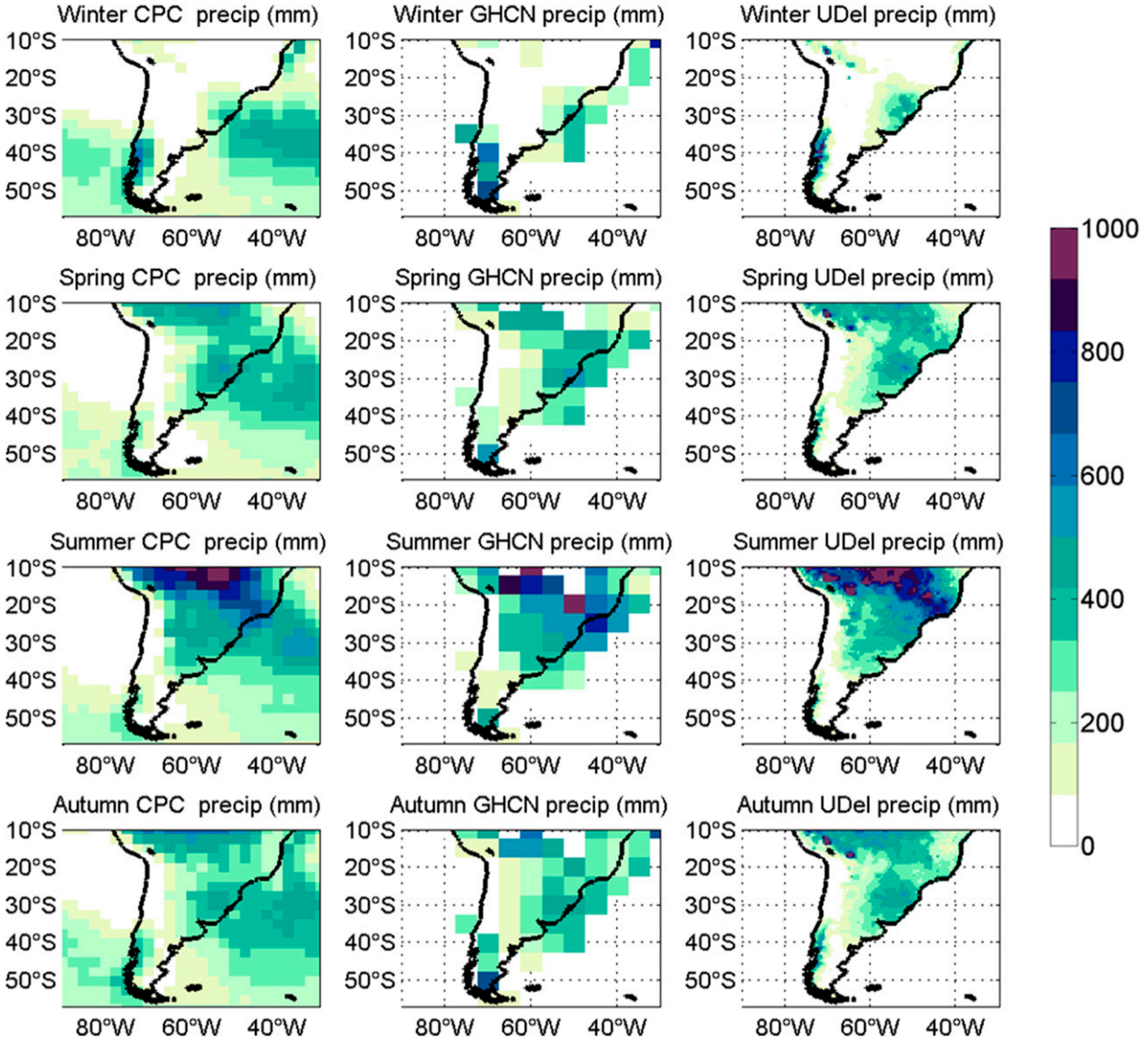

FIG. 2. Seasonal mean precipitation (mm) for (left) CMAP, (center) GHCN, and (right) University of Delaware, from 1980 to 2013.

region (27.5°–57.5°S and 77.5°–67.5°W, indicated by a red box on Fig. 6) with statistically significant correlation between precipitation and the SPH intensity was averaged seasonally, and then SPH intensity, latitude, and longitude were used in a multiple linear regression to determine which combination of these variables best explained interannual variation of precipitation in the subset region. We selected the GHCN (land based) dataset for this correlation analysis. While the GHCN dataset has known errors, including potential biases that could have the most impact on multidecadal precipitation variations (Smith et al. 2012), it has been used successfully to analyze large-scale variability of precipitation, both globally (e.g., van Oldenborgh and Burgers 2005) and in South America (e.g., Garreaud 2009).

Finally, to compare the relationship between the SPH and precipitation with ENSO and precipitation, monthly values of five measures of ENSO were correlated to monthly mean precipitation in the subset region: the Southern Oscillation index (available in real time from http://www.cpc.ncep.noaa.gov/data/indices/soi), the Niño-1+2, Niño-3.4, and Niño-4 indices (available in real time from http://www.cpc.ncep.noaa.gov/data/indices/sstoi.indices), and the multivariate ENSO index (MEI; Wolter and Timlin 1993, 1998).

3. Results

The first significant result of this study is the relationship between precipitation in Chile and the SPH for all months

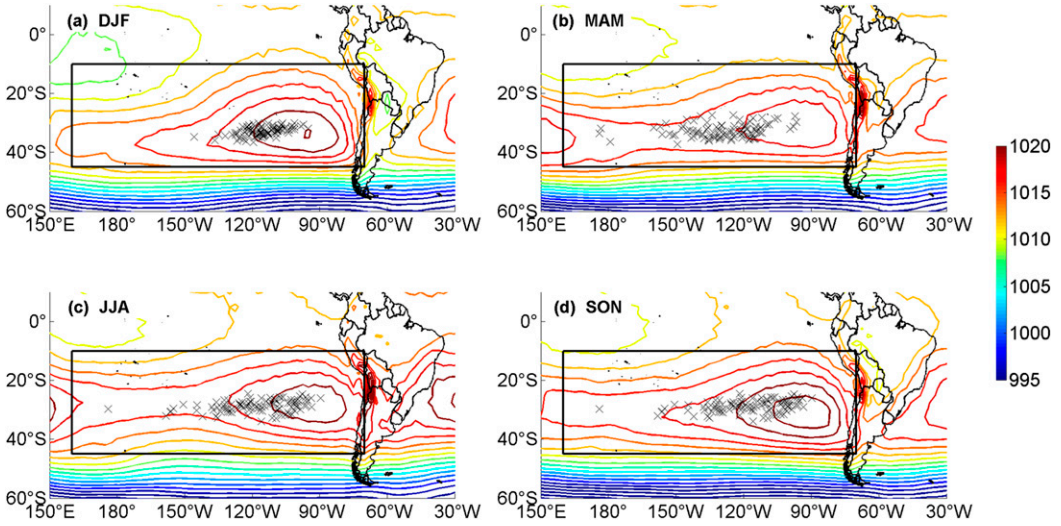

FIG. 3. Seasonal average MSLP (color contours, hPa) and monthly SPH locations (marked with x) from 1980 to 2013 in (a) summer (DJF), (b) autumn (MAM), (c) winter (JJA), and (d) spring (SON). Domain used for calculating SPH mass-weighted centers denoted by black rectangles.

(e.g., not stratifying by season). Statistically significant (at the 5% significance level) Pearson product-moment correlation coefficients were found between all three gridded monthly precipitation datasets and all three measures of the SPH (Fig. 5). Monthly precipitation from 30° to 55°S was negatively correlated with monthly intensity of the SPH (Figs. 5a,d,g), meaning that in months when the SPH was stronger, monthly precipitation over this area was lower. All three precipitation datasets showed this relationship over land, and the CPC dataset indicated that the negative relationship with SPH intensity extended west-northwest over 2000 km into the southeast Pacific Ocean. Correlation coefficients on land, over central and south-central Chile, ranged from −0.20 to −0.40, with the most negative correlation seen at 45°S. (For all results in this section, with a sample size of $n = 34$, correlation coefficients greater than 0.33 are statistically significantly different from zero with 95% confidence.) Similar negative correlations were found between Chilean precipitation and the longitude of the SPH (Figs. 5b,e,h), although CPC precipitation data indicated this relationship was primarily confined to land. In months when the SPH was centered farther to the east (and thus longitude was more positive), monthly precipitation was lower. Correlation coefficients for this relationship ranged between −0.20 and −0.30, with the most negative correlation seen at 35°S. The strongest relationship between monthly precipitation and the SPH, as evidenced by correlation coefficients ranging from 0.30 to 0.60, was found for the latitude of the SPH (Figs. 5c,f,i). In months when the SPH was farther north, monthly precipitation was higher. The most positive correlation coefficient over land (0.60) was found in south-central Chile at 40°S, and this positive relationship extended over 2000 km to the west along 40°S and north to nearly 20°S (Fig. 5c). Although not the focus of this study, strongly negative correlation coefficients (as negative as −0.70) were seen over much of the rest of South America, from eastern Argentina to much of Brazil, Peru, Bolivia, and Ecuador. This dipole in relationship to the latitude of the SPH, with more precipitation in Chile when the SPH is farther north but less precipitation over much of the rest of South America when the SPH is farther north, suggests that the SPH is connected to the large-scale patterns controlling precipitation across much of the continent.

To further explore the relationships between Chilean precipitation and the SPH, and to examine seasonality in the annual relationships, correlation coefficients were calculated individually for four seasons: December–February (DJF), March–May (MAM), June–August (JJA), and September–November (SON). In winter (JJA), correlation patterns between monthly precipitation and SPH intensity (Figs. 6a,d,g) and longitude (Figs. 6b,e,h) most closely resembled the annual patterns discussed above (Fig. 5). Negative correlations between SPH and longitude were found in central Chile, between 30° and 45°S, indicating that winter precipitation was higher when the SPH was weaker and when it was centered farther west. However, unlike the annual pattern, correlations between SPH latitude and winter precipitation (Figs. 6c,f,i) were mostly statistically insignificant over land. Only correlations over the ocean, extending westward along 40°S (Fig. 6c), were found to be positive and statistically significant, indicating that precipitation over the southeast

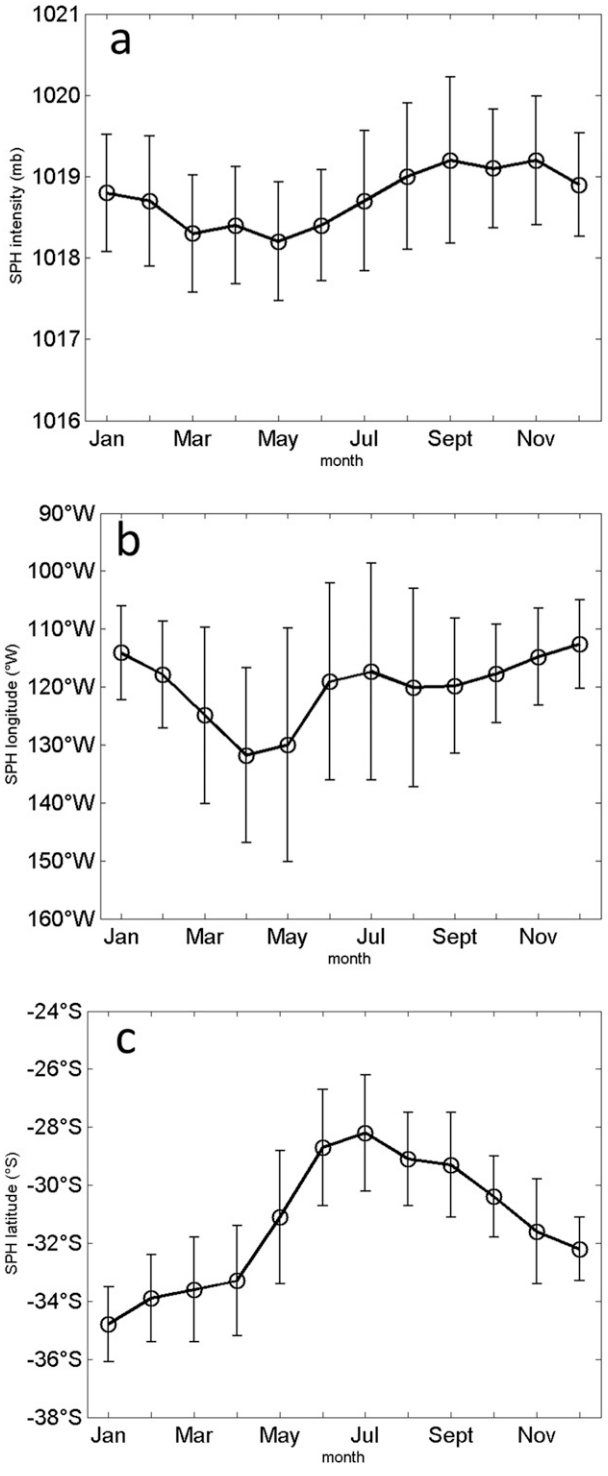

FIG. 4. Monthly mean (black curve and circles) and variability (one standard deviation above and below the mean value) of (a) SPH intensity (hPa), (b) SPH longitude, and (c) SPH latitude for 1980–2013.

Pacific Ocean to the west of the continent increased when the SPH was centered farther north. In spring (SON), correlation coefficients between monthly precipitation and monthly SPH intensity (Figs. 7a,d,g) were negative over south-central Chile (37°–50°S) and ranged between −0.20 and −0.40, very similar to both the winter and the annual correlation patterns. Mostly small (between −0.1 and 0.1) and statistically insignificant correlations were found between spring precipitation and SPH longitude (Figs. 7b,e,h), indicating that spring precipitation, unlike winter precipitation, has little relationship to the east–west position of the SPH. Stronger, positive correlation coefficients (as large as 0.60) between spring precipitation and the latitude of the SPH were found over central and southern Chile (32°–55°S; Figs. 7c,f,i). These correlation coefficients indicated that spring precipitation was higher in months when the SPH was centered farther north, and this was a pattern not seen in winter over land (Figs. 6c,f,i). In summer months (DJF), near-zero and statistically insignificant correlations were found between precipitation and SPH intensity (Figs. 8a,d,g) and SPH longitude (Figs. 8b,e,h) over central and southern Chile. However, positive correlation coefficients (between 0.30 and 0.50) were found over south-central Chile (35°–50°S) between summer precipitation and latitude of the SPH. Thus, similar to spring precipitation, summer precipitation is higher when the SPH is located farther north. In autumn months (MAM), correlation patterns between precipitation and all three SPH metrics more closely resembled those seen in winter. For example, negative correlations (from −0.20 to −0.40) were found over central Chile (35°–45°S) between precipitation and both SPH intensity (Figs. 9a,d,g) and SPH longitude (Figs. 9b,e,h). These relationships indicate that monthly autumn precipitation was greater in months when the SPH was weaker and when it was centered farther west. Also similar to winter, positive correlations (0.30–0.50) between monthly autumn precipitation and SPH latitude were seen from 30° to 55°S (Figs. 9c,f,i), indicating that precipitation was greater in months when the SPH was centered farther north.

The next portion of this study explored the ability to hindcast seasonal precipitation over central and south-central Chile using the three SPH metrics as predictors. Mean monthly precipitation in this region (the region is indicated by a red box in Fig. 6d) was calculated by averaging gridded precipitation values from the GHCN dataset. While winter season was the initial focus because that is when the majority of precipitation in central and south-central Chile occurs and the winter season has the greatest influence from El Niño–Southern Oscillation, we extended the correlation analysis for all seasons to show the influence of the SPH throughout the year. In winter,

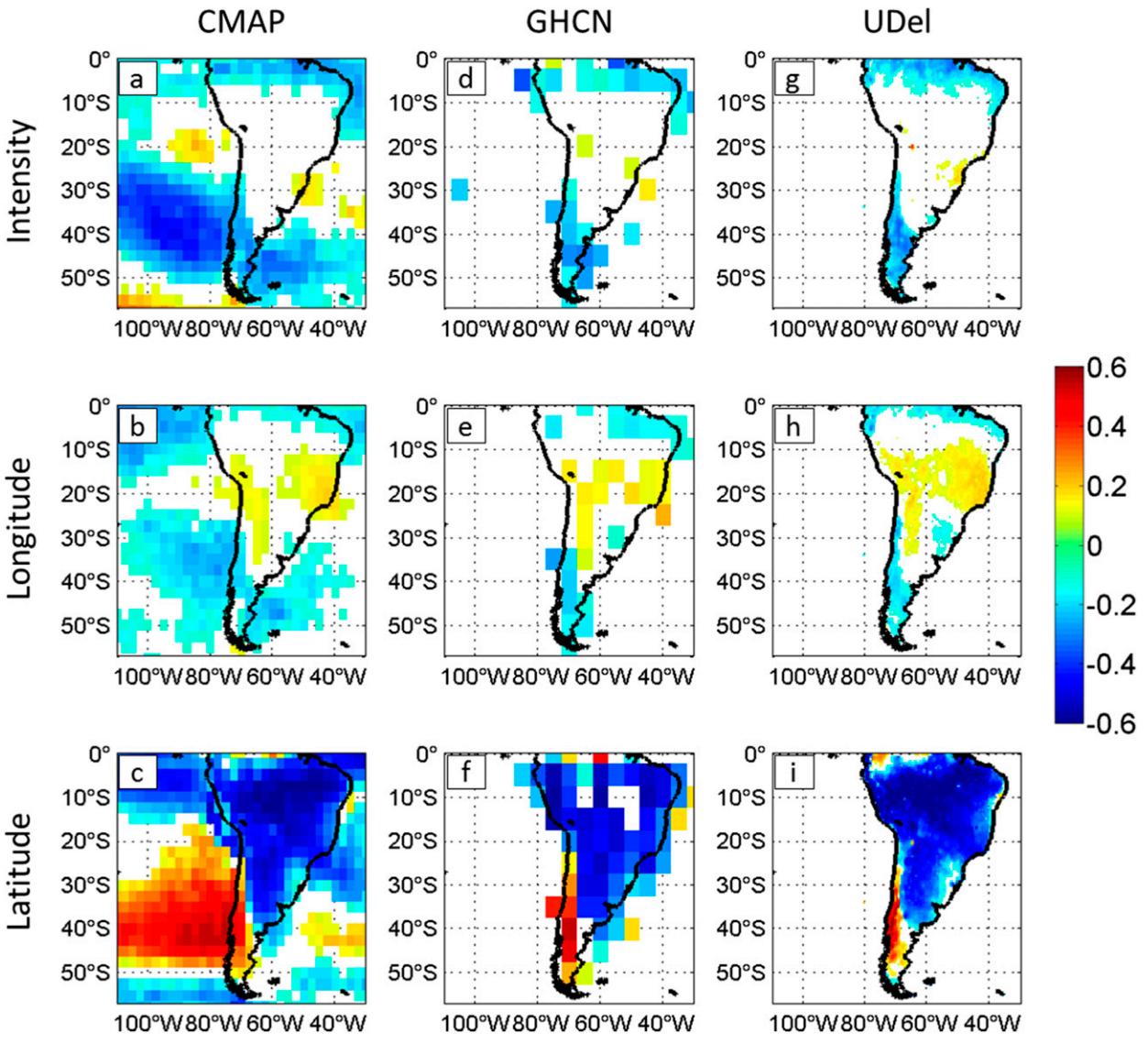

FIG. 5. Pearson product-moment correlation coefficients between monthly CMAP, GHCN, and University of Delaware gridded precipitation and intensity, longitude, and latitude of the SPH for all months of the year. Correlation coefficients between gridded monthly CPC precipitation and monthly values of SPH (a) intensity, (b) longitude, and (c) latitude; (d)–(f) as in (a)–(c), but for GHCN; and (g)–(i) as in (a)–(c), but for the University of Delaware.

summer, and autumn, two of the three SPH metrics had statistically significant correlation coefficients r with precipitation in the subregion: SPH intensity ($r = -0.53$, -0.53, and -0.58, respectively) and SPH longitude ($r = -0.53$, 0.47, and -0.34, respectively) (Table 1). Physically, negative correlations between precipitation and SPH intensity indicate that more precipitation occurs in seasons when the SPH was weaker. In winter and autumn, negative correlations between precipitation and SPH longitude indicate that precipitation is lower in seasons when the SPH is closer to South America (e.g., located farther east). The positive correlation between the anticyclone longitude position and precipitation in summer is interesting, suggesting that summer precipitation—which is often convective and located over the Andes Cordillera—is enhanced when the anticyclone is located closer to South America. In spring, two of the three SPH metrics also had statistically significant correlation coefficients with precipitation: SPH intensity ($r = -0.69$) and SPH latitude ($r = 0.40$) (Table 1). These correlations confirm that spring precipitation is larger when the SPH is weaker and displaced farther north.

In winter, the SPH intensity and longitude metrics compare favorably with the Southern Oscillation index

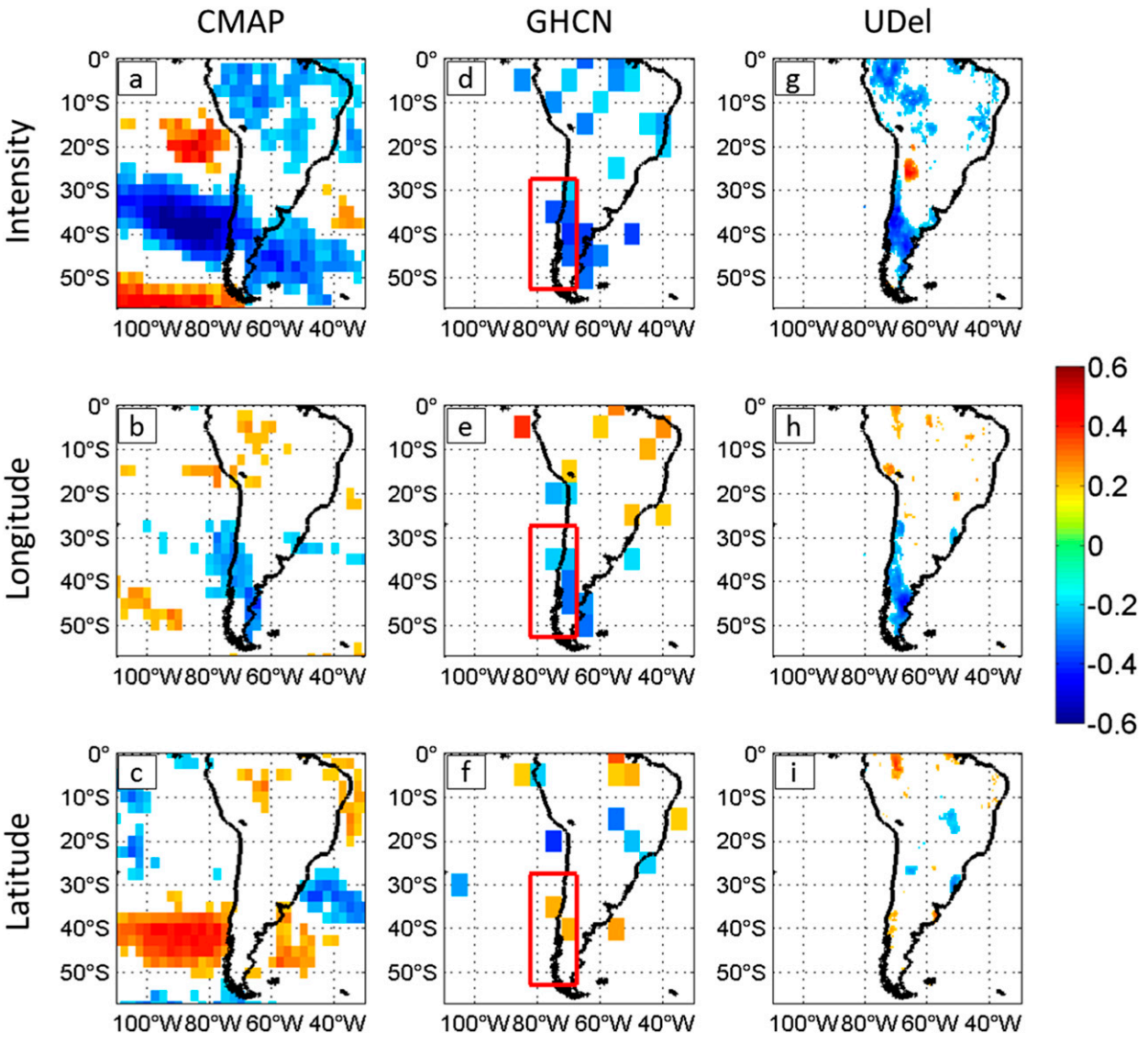

FIG. 6. As in Fig. 5, but for winter (JJA) month correlations between precipitation SPH (a),(d),(g) intensity, (b),(e),(h) latitude, and (c),(f),(i) longitude. Red box in (d)–(f) indicates subregion used to calculate mean winter precipitation for multiple linear regression analysis.

(SOI), which was also statistically significantly correlated to precipitation over the subregion ($r = -0.60$). The correlation of SPH latitude to precipitation was small ($r = 0.14$) and not statistically significant. Because of these correlations, multiple linear regression was performed using intensity and longitude as predictors (Fig. 10). It is important to note that SPH intensity and SPH longitude are uncorrelated, meaning they were independent predictors. Together, monthly SPH intensity and longitude combined to hindcast monthly precipitation with a goodness of fit (R^2) of 0.51. This goodness of fit coefficient is significantly higher than the goodness of fit for the SOI alone ($R^2 = 0.36$). The difference in these coefficients indicates that characteristics of the South Pacific high, specifically its intensity and longitude, can combine to better explain variability in winter-season precipitation over central and south-central Chile than a metric of El Niño–Southern Oscillation.

To better understand the large-scale patterns that are associated with changes in the SPH during winter, composite differences were calculated for the following: 1) winter months with SPH intensity one standard deviation below the winter mean minus years with SPH intensity one standard deviation above the winter mean (Figs. 11a,c) and 2) winter months with SPH longitude one standard deviation below the winter mean

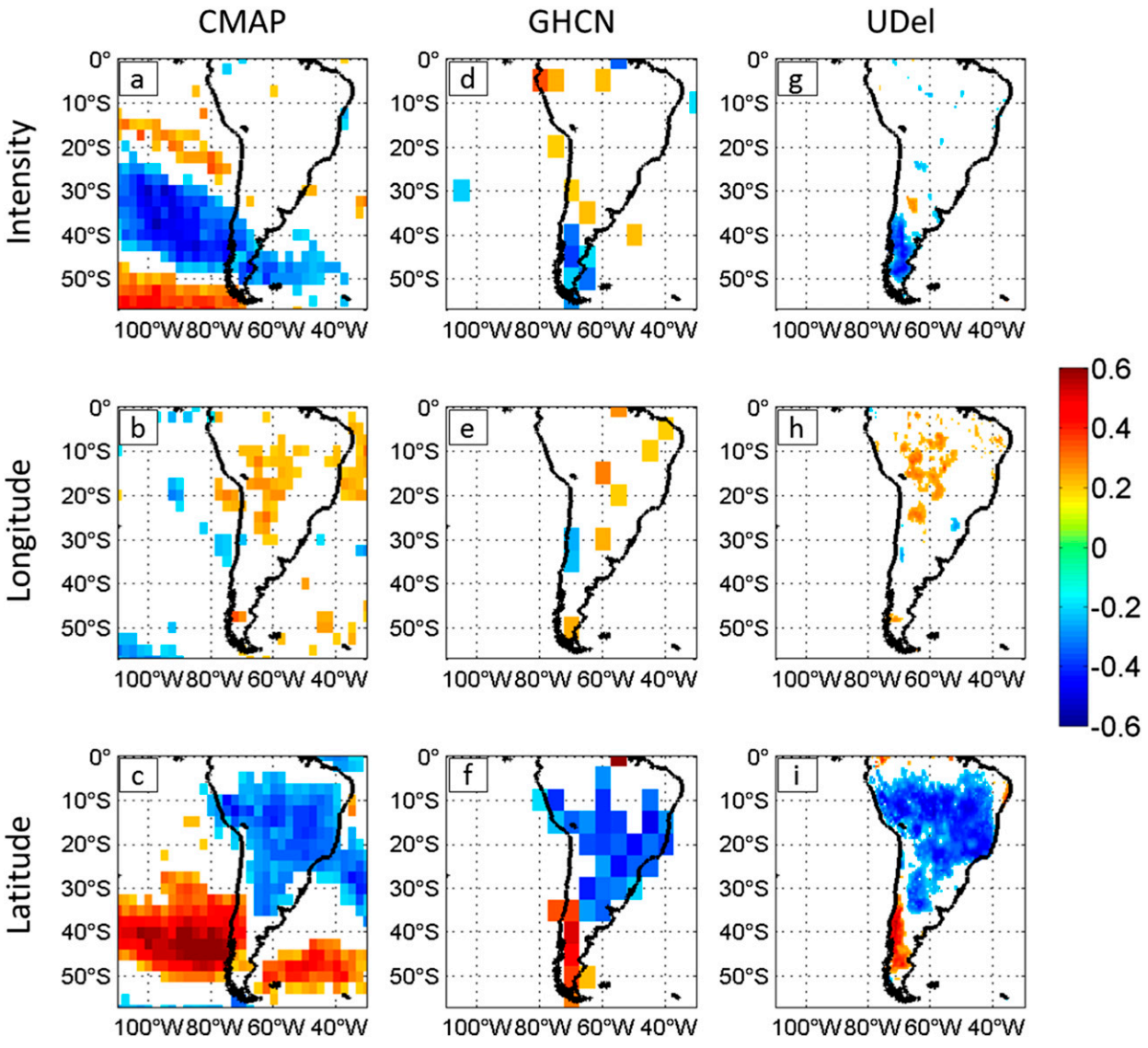

FIG. 7. As in Fig. 5, but for spring (SON).

minus years with SPH longitude one standard deviation above the winter mean (Figs. 11b,d). Composites were calculated for mean sea level pressure (MSLP) and 10-m horizontal wind (Figs. 11a,b) and 850-hPa vertical velocity ω and 850-hPa horizontal wind (Figs. 11c,d). In months when the SPH was weaker, both 10-m and 850-hPa winds were anomalously northerly (anomalously cyclonic) along much of the Chilean coast (20°–50°S) (Figs. 11a,c). Months with a westward-displaced SPH also featured anomalous northerly flow along the Chilean coast from 30° to 50°S, albeit somewhat weaker in magnitude (Figs. 11b,d). Northerly anomalous surface flow is a pattern associated with enhanced moisture advection and enhanced rainfall over Chile (Falvey and Garreaud 2007). Thus, this physical pattern supports the observed negative correlations between winter precipitation and SPH intensity and longitude (Fig. 6). In months when the SPH was weaker, 850-hPa vertical velocity was anomalously upward along the coast from 25° to 50°S, a pattern also seen (albeit with smaller magnitudes) in months when the SPH was displaced to the west. This physical pattern supports observed negative correlations between SPH intensity and longitude and winter precipitation.

To complement these physical composites, correlations between winter SPH intensity and three measures of diabatic heating were calculated from the global gridded CFSR, similar to Leonardo and Hameed (2015). Correlation coefficients were examined at 25-hPa increments from 975 to 600 hPa for deep convective heating

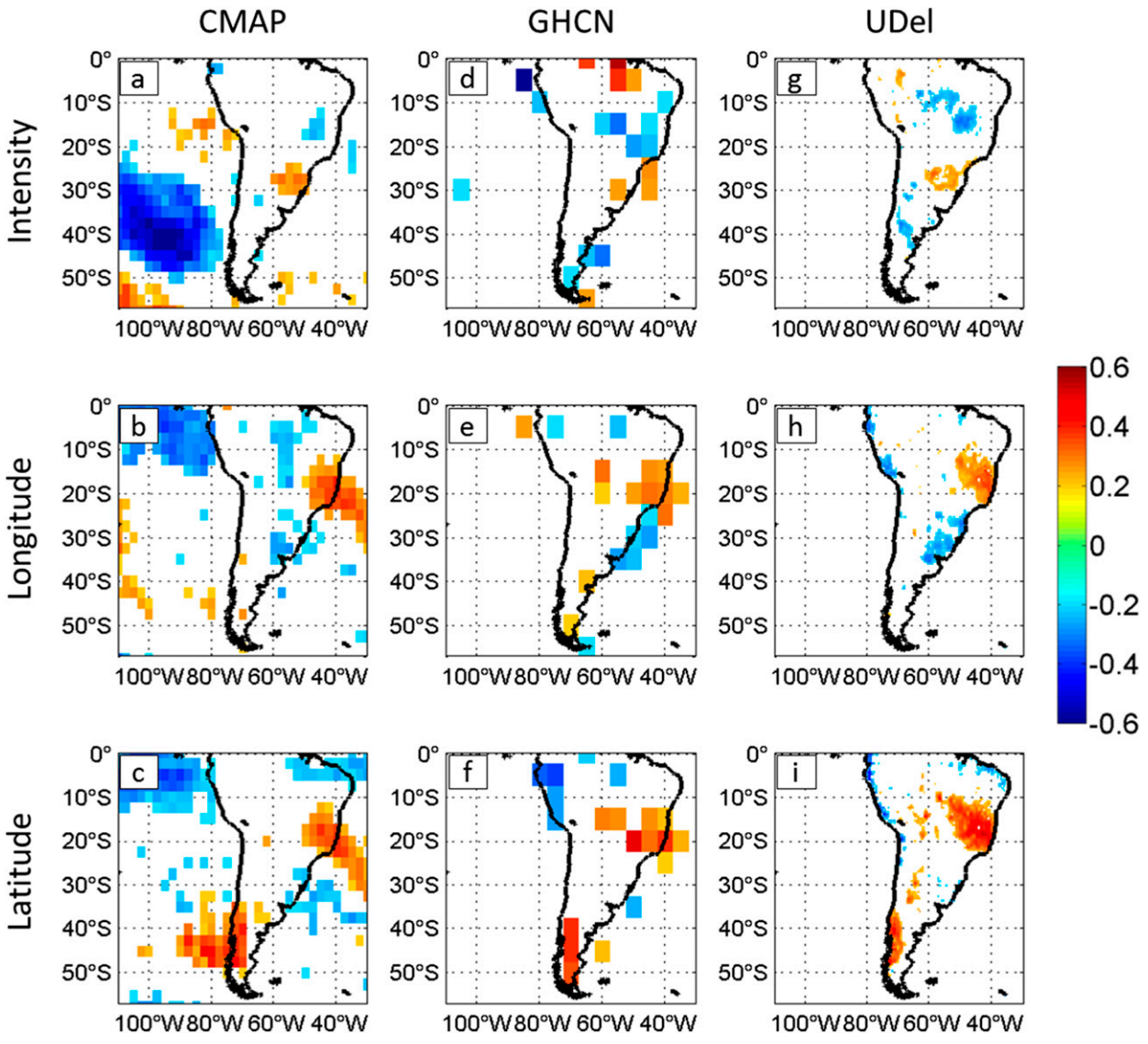

FIG. 8. As in Fig. 5, but for summer (DJF).

rate, shallow convective heating rate, and the large-scale condensate heating rate, and while all 17 pressure levels were examined, only the pressure level with the greatest surface area of statistically significant positive correlations (significant at the 95% confidence level) is presented for each variable. Furthermore, only positive correlations are shown because we are interested in heating that contributes to subsidence and increased SPH pressure. Positive correlations between SPH intensity and deep convective heating rate at 700 hPa show that convection over Indonesia extending southeast along the South Pacific convergence zone (SPCZ; Kiladis et al. 1989; Vincent 1994) contributes to SPH intensity (Fig. 12a). Positive correlations between shallow convective heating rate at 950 hPa and SPH intensity are very similar, suggesting that convection extending from the Indian Ocean monsoon region in JJA to the southeast over Indonesia and also into the SPCZ contributes to subsidence over the SPH region and increased SPH intensity (Fig. 12b). Finally, 950-hPa large-scale condensate heating rates in both the equatorial Pacific and the extratropical southeast Pacific are positively correlated to SPH intensity (Fig. 12c). These three correlation patterns show that SPH intensity is related to convective activity over both the Indian Ocean and Indonesian monsoon regions as well as the equatorial, subtropical (e.g., SPCZ), and extratropical Pacific. These results agree with Rodwell and Hoskins (2001) who proposed that anticyclone circulations to the east of major monsoon circulations were driven by subsidence

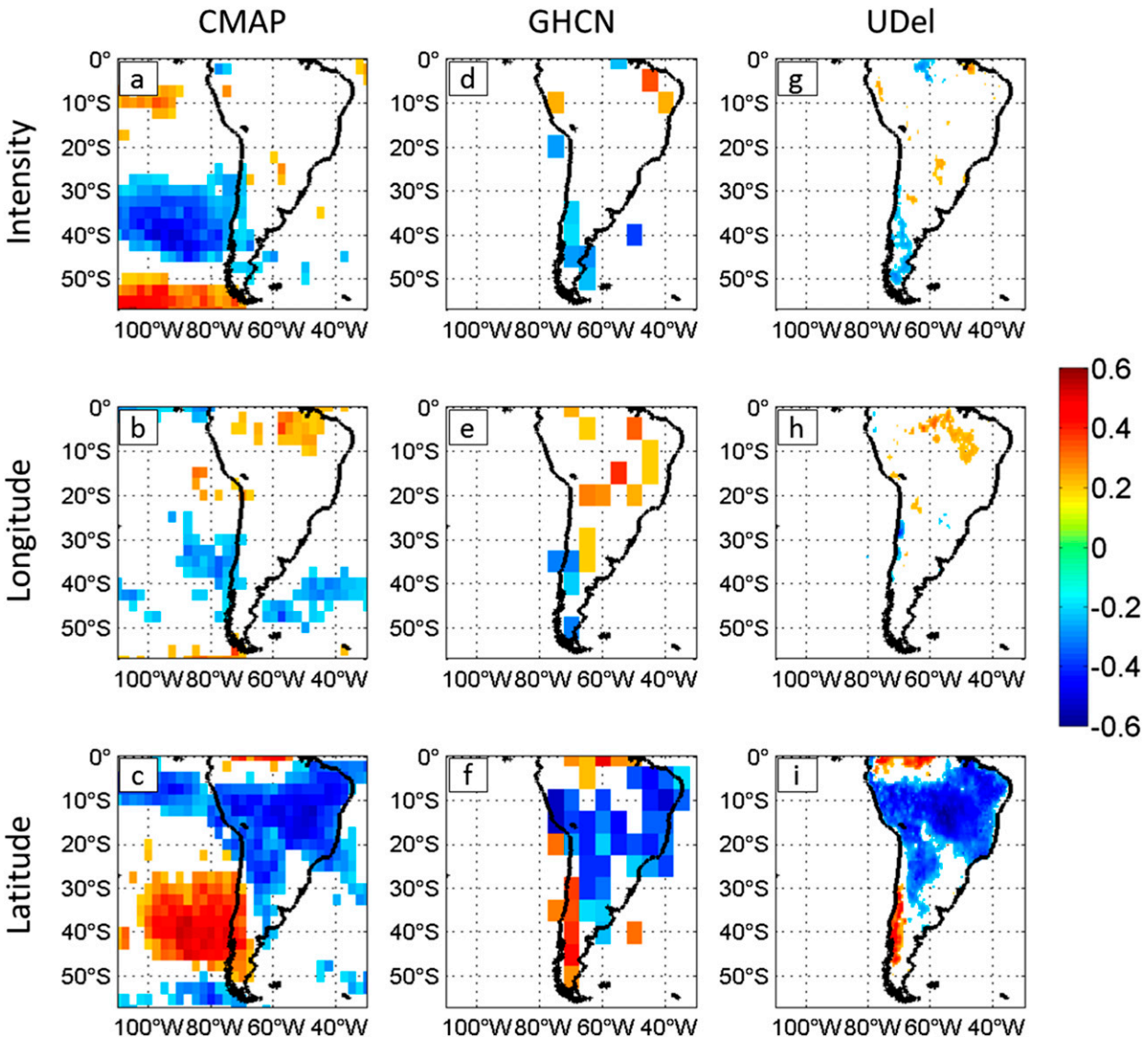

FIG. 9. As in Fig. 5, but for autumn (MAM).

associated with the convective heating of the monsoon precipitation.

ENSO is a coupled atmosphere–ocean system, and it is interesting to ask which of its components is most directly related to precipitation in Chile. To investigate this question we correlated Chile winter precipitation to five different indices of ENSO: (i) SOI, which is the difference in pressure anomalies between Tahiti and Darwin; (ii) MEI, which combines data on atmospheric pressure, surface winds, cloudiness, atmospheric temperature, and sea surface temperature; and (iii) Niño-1+2, (iv) Niño-3.4, and (v) Niño-4, which quantify SST fluctuations in different longitudinal segments of the equatorial Pacific. The correlations of the SST-based indices of ENSO with winter Chilean precipitation are smaller than that of the SOI (Table 2). The SOI is an atmosphere-only index, suggesting that the largest part of the ENSO modulation of Chilean precipitation occurs via the atmosphere. Correlation of MEI with winter Chilean precipitation was smaller than SOI but larger than the SST-only indices, which is not surprising because the MEI captures interannual fluctuations in both the atmosphere and the ocean. These correlation coefficients confirm that the dominant link between ENSO and Chilean precipitation comes primarily via atmospheric processes: the altering of the distribution of atmospheric pressure, specifically in the region of the SPH, which then impacts precipitation.

The correlation coefficients calculated above reflect both direct contributions of the given ENSO index on Chile winter precipitation and indirect contributions

TABLE 1. Correlation coefficients r between winter, spring, summer, and autumn precipitation, respectively, in central and southern Chile (red box in Fig. 5) and the Southern Oscillation index, SPH intensity, SPH longitude, and SPH latitude. Correlations significant at the 0.05 significance level are shown in bold.

	Precipitation	Intensity	Longitude	Latitude	SOI
Winter (JJA)					
Precipitation	**1**				
Intensity	**−0.53**	**1**			
Longitude	**−0.53**	0.1	**1**		
Latitude	0.14	**−0.41**	**0.36**	**1**	
SOI	**−0.60**	**0.54**	**0.36**	0.04	**1**
Spring (SON)					
Precipitation	**1**				
Intensity	**−0.69**	**1**			
Longitude	0.30	**−0.45**	**1**		
Latitude	**0.40**	**−0.55**	0.32	**1**	
SOI	**−0.55**	**0.70**	−0.20	−0.08	**1**
Summer (DJF)					
Precipitation	**1**				
Intensity	**−0.53**	**1**			
Longitude	**0.47**	**−0.45**	**1**		
Latitude	0.27	**−0.45**	**0.56**	**1**	
SOI	−0.22	0.26	−0.10	0.29	**1**
Autumn (MAM)					
Precipitation	**1**				
Intensity	**−0.58**	**1**			
Longitude	**−0.34**	**0.35**	**1**		
Latitude	0.08	**−0.40**	0.28	**1**	
SOI	**−0.38**	**0.53**	**0.52**	−0.10	**1**

from other ENSO indices, which interact with the given ENSO index and Chilean precipitation. To isolate the effects of each ENSO index, we also computed the partial correlation coefficients for the five ENSO indices and Chilean precipitation. The partial correlation coefficients report the contribution from a given ENSO index on precipitation while holding all other independent variables fixed. The partial correlation of SOI and Chilean precipitation is −0.49 and is statistically significant, with $p < 0.05$ level. Partial correlations of Chile winter precipitation and MEI, Niño-3.4, Niño-4, and Niño-1+2 are −0.23, 0.27, −0.25, and 0.18, respectively, and all are not statistically significant. This result shows that the teleconnection between ENSO and Chilean precipitation occurs within the atmosphere as changes in atmospheric pressure characterized by SOI perturb the distribution of pressures in the SPH region. That the correlation between winter precipitation and combined SPH intensity and longitude is higher than SOI, MEI, or any of the SST-only-based indices confirms that the SPH explains more of the variability in winter precipitation than ENSO alone. Furthermore, this pattern was seen in all seasons, not only winter, including the summer season when the SOI is insignificantly correlated with precipitation. The SPH thus plays an important role in controlling Chilean precipitation variability throughout the year.

4. Discussion and conclusions

The seasonal correlation patterns seen in Figs. 5–8 explain the annual patterns seen in Fig. 4. For example, annually, precipitation over central and south-central

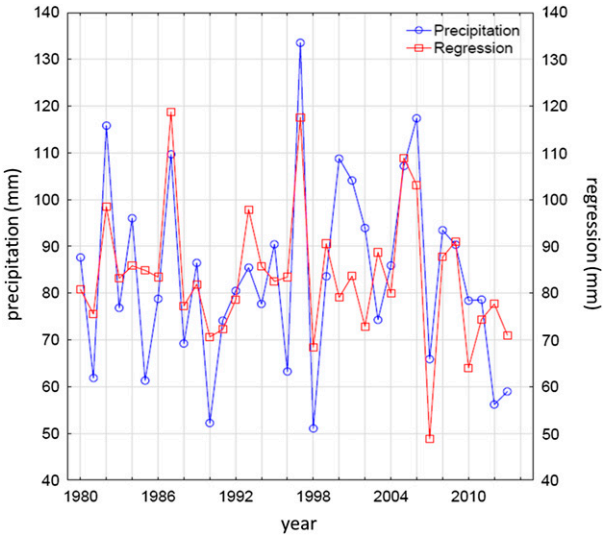

FIG. 10. Mean precipitation (blue) and multiple linear regression of precipitation (red) in central and south-central Chile, the region indicated by a red box region in Fig. 6. Multiple linear regression used SPH intensity and longitude as predictors.

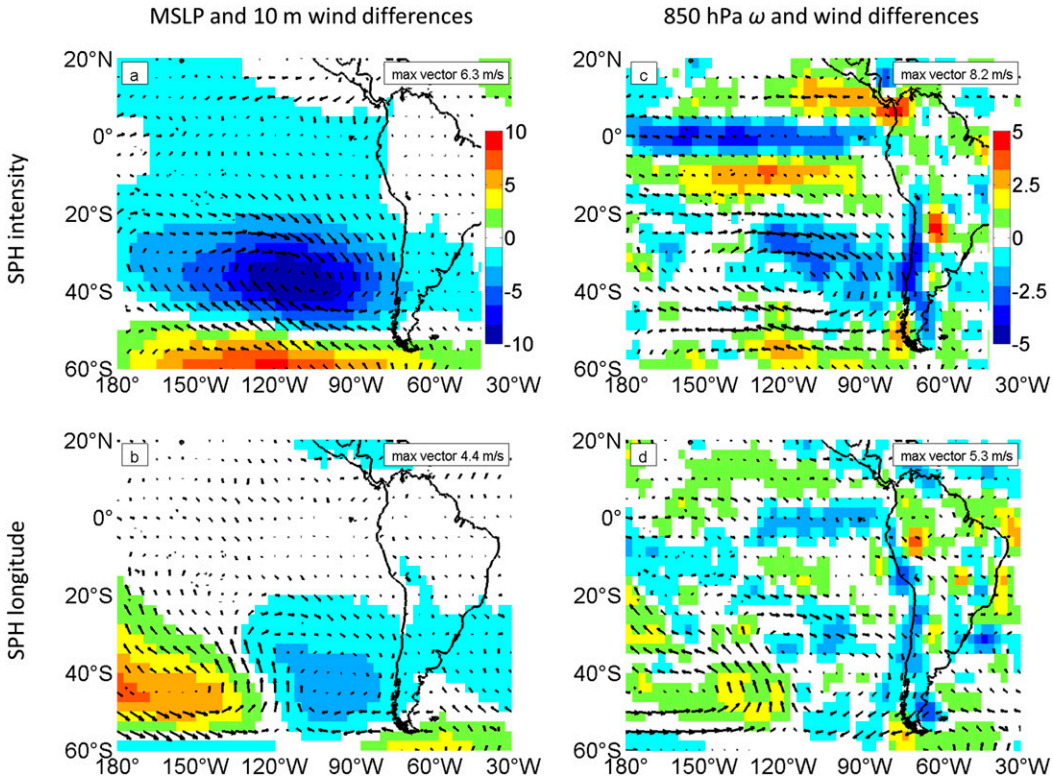

FIG. 11. Differences in winter (JJA) (a),(b) sea level pressure (hPa) and 10-m wind (vector) and (c),(d) 850-hPa vertical velocity (hPa s^{-1}) and 850-hPa wind (vector). Differences shown in (a),(c) were calculated by subtracting the winter mean for years when SPH intensity was more than one standard deviation above normal (1988, 1998, 2007, and 2010) from the winter mean for years when SPH intensity was more than one standard deviation below normal (1982, 1986, 1997, 2005, and 2006). Differences shown in (b),(d) were calculated by subtracting the winter mean for years when SPH longitude was more than one standard deviation above normal (1986, 1990, 1991, and 2002) from the winter mean for years when SPH longitude was more than one standard deviation below normal (1987, 1993, 1997, and 2005).

Chile is negatively correlated to the intensity and longitude of the SPH and positively correlated to the latitude of the SPH. However, the negative correlations to SPH intensity were only seen in winter (Fig. 5), spring (Fig. 6), and autumn (Fig. 8), and the negative correlations to SPH longitude were only seen in winter and autumn. Furthermore, the positive correlation to latitude was seen over land stations only in spring, summer (Fig. 7), and autumn and largely absent in winter. The results of a multiple linear regression confirmed the importance of two SPH metrics (intensity and longitude) and the unimportance of a third SPH metric (latitude) in hindcasting winter precipitation in central and south-central Chile. Based on the synoptic-scale controls on precipitation discussed in Montecinos et al. (2000), Garreaud (2009), Montecinos and Aceituno (2003), Barrett et al. (2009), Viale and Nuñez (2011), and Catto et al. (2012), the following physical mechanisms are proposed to explain the observed correlations. In winter, and to a lesser extent spring and autumn, precipitation is mostly a result of frontal passages and moisture advection associated with midlatitude cyclones. As such, a weaker and westward-displaced SPH would allow for greater precipitation from these low pressure systems. Additionally, in winter, the SPH is climatologically already displaced relatively far to the north (Fig. 4b), reducing its relative influence of variability in its latitude on midlatitude cyclones and yielding the observed weak correlations between SPH latitude and winter precipitation. However, in spring, summer, and autumn, variability in the SPH latitude exerts relatively more control on the static stability of the atmosphere, a component necessary for convective precipitation in those three seasons. In summer, the longitude of the SPH is relatively unimportant to precipitation, likely a result of its tighter geographic clustering (Fig. 4a) than seen in the other three seasons (Figs. 4b–d).

Finally, it has been noted in successive IPCC reports that global climate models can reproduce large-scale features of atmospheric circulation with some reliability, but simulation of regional climate remains a difficult problem, and therefore little confidence can be placed

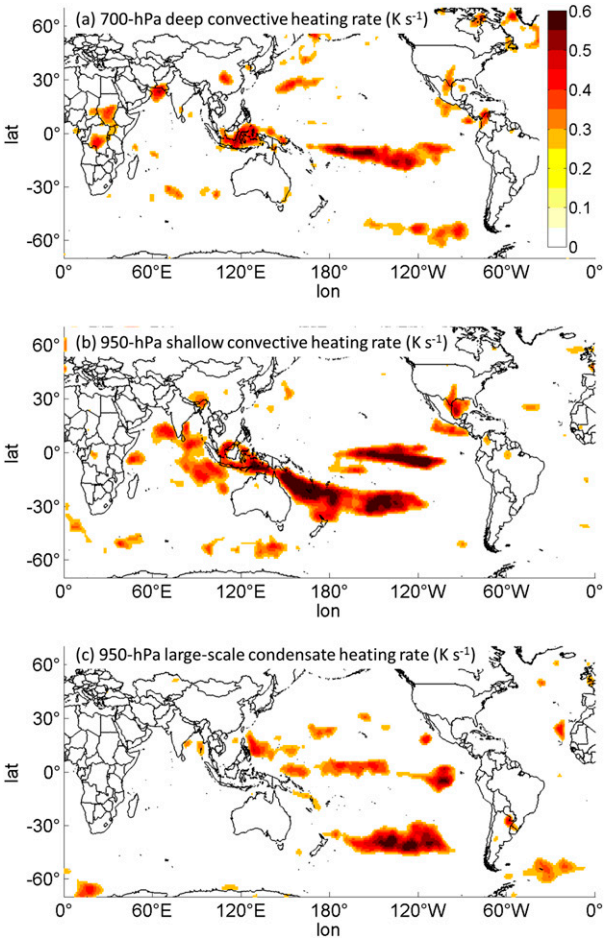

FIG. 12. Correlation coefficients r between (a) 700-hPa deep convective heating rate ($K\,s^{-1}$), (b) 950-hPa shallow convective heating rate ($K\,s^{-1}$), and (c) 950-hPa large-scale condensate heating rate ($K\,s^{-1}$). Only positive correlations significant at $p \leq 0.05$ are shown.

in predictions of changes expected under global warming scenarios for a small region such as Chile (IPCC 2015; Trenberth and Asrar 2014). The results presented in this paper offer a pathway to diagnosing the impact of global climate change on Chilean precipitation in the future (i.e., by examination of the South Pacific high in the GCMs). The SPH, like other subtropical highs, is a large-scale permanent feature of atmospheric circulation. Its genesis is in the subsidence of air in the subtropical South Pacific. A climate model's success in describing changes in Chilean precipitation is related to the accuracy in the simulation of physical processes that determine the pressure and position of the SPH. Therefore, studies like this one, a quantitative comparison of pressure and position of the high with those in reanalysis data, can shed light on model skill in calculating regional rainfall in Chile and projecting these quantities into the future.

TABLE 2. Correlation coefficients r between winter precipitation in central and southern Chile (red box in Fig. 6) and different El Niño–Southern Oscillation indices.

SOI	−0.60
MEI	0.52
Niño-1+2	0.35
Niño-3.4	0.48
Niño-4	0.36

Acknowledgments. The authors thank the anonymous reviewers for their comments, which helped strengthen the manuscript. Author B. Barrett acknowledges partial financial support from the Fulbright Scholar Program.

REFERENCES

Aceituno, P., 1988: On the functioning of the Southern Oscillation in the South American sector. Part I: Surface climate. *Mon. Wea. Rev.*, **116**, 505–524, doi:10.1175/1520-0493(1988)116<0505:OTFOTS>2.0.CO;2.

——, and A. Montecinos, 1993: Stability analysis of the relation between the Southern Oscillation and rainfall in South America (in Spanish). *Bull. Inst. Fr. Etudes Andines*, **22**, 53–61.

Barrett, B. S., R. Garreaud, and M. Falvey, 2009: Effect of the Andes Cordillera on precipitation from a midlatitude cold front. *Mon. Wea. Rev.*, **137**, 3092–3109, doi:10.1175/2009MWR2881.1.

Catto, J. L., C. Jakob, G. Berry, and N. Nicholls, 2012: Relating global precipitation to atmospheric fronts. *Geophys. Res. Lett.*, **39**, L10805, doi:10.1029/2012GL051736.

Chen, M., P. Xie, J. E. Janowiak, and P. A. Arkin, 2002: Global land precipitation: A 50-yr monthly analysis based on gauge observations. *J. Hydrometeor.*, **3**, 249–266, doi:10.1175/1525-7541(2002)003<0249:GLPAYM>2.0.CO;2.

Falvey, M., and R. Garreaud, 2007: Wintertime precipitation episodes in central Chile: Associated meteorological conditions and orographic influences. *J. Hydrometeor.*, **8**, 171–193, doi:10.1175/JHM562.1.

Fuenzalida, H., 1982: A country of extreme climate (in Spanish). *Chile: Essence and Evolution*, H. Garcia, Ed., Instituto de Estudios Regionales, Universidad de Chile, 27–35.

Garreaud, R. D., 1995: Configuraciones atmosféricas durante tormentas pluviales en Chile central. *Meteorológica*, **19**, 73–81.

——, 2009: The Andes climate and weather. *Adv. Geosci.*, **7**, 1–9.

Grimm, A. M., V. R. Barros, and M. E. Doyle, 2000: Climate variability in southern South America associated with El Niño and La Niña events. *J. Climate*, **13**, 35–58, doi:10.1175/1520-0442(2000)013<0035:CVISSA>2.0.CO;2.

Grotjahn, R., 2004: Remote weather associated with South Pacific subtropical sea-level high properties. *Int. J. Climatol.*, **24**, 823–839, doi:10.1002/joc.1024.

Hameed, S., M. J. Iqbal, S. Rehman, and D. Collins, 2011: Impact of the Indian Ocean high pressure system on winter precipitation over western and southwestern Australia. *Aust. Meteor. Oceanogr. J.*, **61**, 159–170.

IPCC, 2015: Representing regional projection uncertainty using sub-sets of CMIP5. *IPCC Workshop on Regional Climate Projections and Their Use in Impacts and Risk Analysis Studies*, São José dos Campos, Brazil, IPCC, 130–131. [Available online at https://www.ipcc.ch/pdf/supporting-material/RPW_WorkshopReport.pdf.]

Kalnay, E., and Coauthors, 1996: The NCEP/NCAR 40-Year Reanalysis Project. *Bull. Amer. Meteor. Soc.*, **77**, 437–471, doi:10.1175/1520-0477(1996)077<0437:TNYRP>2.0.CO;2.

Karoly, D. J., 1989: Southern Hemisphere circulation features associated with El Niño–Southern Oscillation events. *J. Climate*, **2**, 1239–1252, doi:10.1175/1520-0442(1989)002<1239:SHCFAW>2.0.CO;2.

Kiladis, G. N., H. V. Storch, and H. V. Loon, 1989: Origin of the South Pacific convergence zone. *J. Climate*, **2**, 1185–1195, doi:10.1175/1520-0442(1989)002<1185:OOTSPC>2.0.CO;2.

Legates, D. R., and C. J. Willmott, 1990: Mean seasonal and spatial variability in gauge-corrected, global precipitation. *Int. J. Climatol.*, **10**, 111–127, doi:10.1002/joc.3370100202.

Leonardo, N., and S. Hameed, 2015: Impact of the Hawaiian high on interannual variations of winter precipitation over California. *J. Climate*, **28**, 5667–5682, doi:10.1175/JCLI-D-14-00518.1.

Montecinos, A., 1998: Seasonal rainfall forecast in central Chile (in Spanish). M.S. thesis, Department of Geophysics, University of Chile, 116 pp.

——, and P. Aceituno, 2003: Seasonality of the ENSO-related rainfall variability in central Chile and associated circulation anomalies. *J. Climate*, **16**, 281–296, doi:10.1175/1520-0442(2003)016<0281:SOTERR>2.0.CO;2.

——, A. Díaz, and P. Aceituno, 2000: Seasonal diagnostic and predictability of rainfall in subtropical South America based on tropical Pacific SST. *J. Climate*, **13**, 746–758, doi:10.1175/1520-0442(2000)013<0746:SDAPOR>2.0.CO;2.

Peterson, T. C., and R. S. Vose, 1997: An overview of the Global Historical Climatology Network temperature database. *Bull. Amer. Meteor. Soc.*, **78**, 2837–2849, doi:10.1175/1520-0477(1997)078<2837:AOOTGH>2.0.CO;2.

Pittock, A. B., 1980: Patterns of climatic variation in Argentina and Chile—I. Precipitation, 1931–60. *Mon. Wea. Rev.*, **108**, 1347–1361, doi:10.1175/1520-0493(1980)108<1347:POCVIA>2.0.CO;2.

Pizarro, R., and Coauthors, 2012: Latitudinal analysis of rainfall intensity and mean annual precipitation in Chile. *Chil. J. Agric. Res.*, **72**, 252–261, doi:10.4067/S0718-58392012000200014.

Rodwell, M. J., and B. J. Hoskins, 2001: Subtropical anticyclones and summer monsoons. *J. Climate*, **14**, 3192–3211, doi:10.1175/1520-0442(2001)014<3192:SAASM>2.0.CO;2.

Rutllant, J., and H. Fuenzalida, 1991: Synoptic aspects of the central Chile rainfall variability associated with the Southern Oscillation. *Int. J. Climatol.*, **11**, 63–76, doi:10.1002/joc.3370110105.

Saha, S., and Coauthors, 2010: The NCEP Climate Forecast System Reanalysis. *Bull. Amer. Meteor. Soc.*, **91**, 1015–1057, doi:10.1175/2010BAMS3001.1.

Smith, T. M., P. A. Arkin, L. Ren, and S. S. P. Shen, 2012: Improved reconstruction of global precipitation since 1900. *J. Atmos. Oceanic Technol.*, **29**, 1505–1517, doi:10.1175/JTECH-D-12-00001.1.

Trenberth, K. E., and G. R. Asrar, 2014: Challenges and opportunities in water cycle research: WCRP contributions. *Surv. Geophys.*, **35**, 515–532, doi:10.1007/s10712-012-9214-y.

van Oldenborgh, G. J., and G. Burgers, 2005: Searching for decadal variations in ENSO precipitation teleconnection. *Geophys. Res. Lett.*, **32**, L15701, doi:10.1029/2005GL023110.

Verbist, K., A. W. Robertson, W. M. Cornelis, and D. Gabriels, 2010: Seasonal predictability of daily rainfall characteristics in central-northern Chile for dry-land management. *J. Appl. Meteor. Climatol.*, **49**, 1938–1955, doi:10.1175/2010JAMC2372.1.

Viale, M., and M. N. Nuñez, 2011: Climatology of winter orographic precipitation over the subtropical central Andes and associated synoptic and regional characteristics. *J. Hydrometeor.*, **12**, 481–507, doi:10.1175/2010JHM1284.1.

——, and R. Garreaud, 2015: Orographic effects of the subtropical and extratropical Andes on upwind precipitating clouds: Effects of the Andes on precipitation. *J. Geophys. Res. Atmos.*, **120**, 4962–4974, doi:10.1002/2014JD023014.

——, R. Houze Jr., and K. Rasmussen, 2013: Upstream orographic enhancement of a narrow cold-frontal rainband approaching the Andes. *Mon. Wea. Rev.*, **141**, 1708–1730, doi:10.1175/MWR-D-12-00138.1.

Vincent, D. G., 1994: The South Pacific convergence zone (SPCZ): A review. *Mon. Wea. Rev.*, **122**, 1949–1970, doi:10.1175/1520-0493(1994)122<1949:TSPCZA>2.0.CO;2.

Wolter, K., and M. S. Timlin, 1993: Monitoring ENSO in COADS with a seasonally adjusted principal component index. *Proc. 17th Climate Diagnostics Workshop*, Norman, OK, NOAA/NMC/CAC, 52–57. [Available online at http://www.esrl.noaa.gov/psd/enso/mei/WT1.pdf.]

——, and ——, 1998: Measuring the strength of ENSO events: How does 1997/98 rank? *Weather*, **53**, 315–324, doi:10.1002/j.1477-8696.1998.tb06408.x.

Wright, J. S., and S. Fueglistaler, 2013: Large differences in reanalyses of diabatic heating in the tropical upper troposphere and lower stratosphere. *Atmos. Chem. Phys.*, **13**, 9565–9576, doi:10.5194/acp-13-9565-2013.

Xie, P., and P. A. Arkin, 1997: Global precipitation: A 17-year monthly analysis based on gauge observations, satellite estimates, and numerical model outputs. *Bull. Amer. Meteor. Soc.*, **78**, 2539–2558, doi:10.1175/1520-0477(1997)078<2539:GPAYMA>2.0.CO;2.